


A novel under-actuated bionic hand and its grasping stability analysis

Advances in Mechanical Engineering
2017, Vol. 9(2) 1–13
© The Author(s) 2017
DOI: 10.1177/1687814016688859
journals.sagepub.com/home/ade


Xin Li¹, Qiang Huang¹, Xuechao Chen¹, Zhangguo Yu¹, Jinying Zhu¹ and Jianda Han²

Abstract

This article presents a novel under-actuated robot hand, which has a thumb and two cooperative fingers. The thumb has two joints with 2 degrees of freedom driven by one motor. Each of the other two fingers has the same mechanism structure with the thumb and forms a cooperative mechanism, which is driven by only one motor with 4 degrees of freedom in total. All the under-actuated fingers are designed with the transmission mechanisms based on a kind of mechanism combined with the linkage mechanism and the passive elements. In this article, it is shown that under-actuated hand is able to reproduce most of the grasping behaviors of the human hand anthropomorphically and self-adaptively, without increasing the complexity of mechanism and control. The grasping stability analysis is given to help to understand the size range and load range of a stable grasp. Finally, the experiment results verify the high efficiency and stability of the novel mechanism.

Keywords

Under-actuated mechanism, linkage mechanism, cooperative mechanism, force analysis, stability analysis

Date received: 6 July 2016; accepted: 11 December 2016

Academic Editor: Yangmin Li

Introduction

For decades, many bionic hands with numerous degrees of freedom (DOFs), small volume, and powerful output have been developed. The research of designing bionic hands is a popular topic since robots need more precise operation with hand in the forthcoming robot age. According to the application, the design of robotic hand can be simply divided into two types, simple hand or gripper for industrial production and dexterous hand for service robot or the upper limb amputee. The former is to reduce or replace the manual operation in industrial manufacturing; the key is focusing on the function and reliability. As the tasks are quite simple, generally there is no consideration in the bionics. The industrial hand may be just a simple gripper, with only one joint for each finger for simplicity, while its main task is to accomplish a simple grasp.

While the dexterous hands are equipped on service robot and humanoid robot where precise operation is

needed. In addition to considering the performance problems, bionics, which means the shape and mass similarity compared with the human body, should also be taken into consideration. Dexterous hands can accomplish some accurate grasp and even precise manipulation. Famous dexterous hands include Stanford/JPL hand,¹ Utah/MIT hand,² Robonaut hand,³ Bebionic hand,⁴ HIT/DLR II,⁵ and the Shadow Hand,⁶ which can provide 24 movements to reproduce as closely as possible the kinematics and dexterity of

¹School of Mechatronical Engineering, Beijing Institute of Technology, Beijing, China

²State key Laboratory of Robotics, Shenyang Institute of Automation, Chinese Academy of Sciences, Shenyang, China

Corresponding author:

Xuechao Chen, Beijing Institute of Technology, No. 5, Zhongguancun South Street, Haidian District, Beijing 100081, China.
Email: chenxuechao@bit.edu.cn



Creative Commons CC-BY: This article is distributed under the terms of the Creative Commons Attribution 3.0 License (<http://www.creativecommons.org/licenses/by/3.0/>) which permits any use, reproduction and distribution of the work without

further permission provided the original work is attributed as specified on the SAGE and Open Access pages (<https://us.sagepub.com/en-us/nam/open-access-at-sage>).

human hand. Dexterous robotic hands have been a perennial research topic, and their goals are almost exclusive to obtain more functions like human hand. However, it has been suggested that using anthropomorphic design approaches is restrictive and ambitious since one tends to copy what nature has produced in millions of years of evolution.⁷ Therefore, compromise between versatility and simplicity should be taken into consideration in order to obtain relevant practical systems,⁸ and the main focus of this article is on how to improve the anthropomorphosis and the grasping stability of the hand.

Under-actuated (UA) mechanism can be regarded as a novel way to improve the anthropomorphosis and grasping stability of hands.^{9,10} A hand is considered to be UA if the number of actuators in the hand is smaller than the number of DOF.¹¹ UA hands have achieved a rapid development in recent years owing to their special characteristics, including the considerable number of joints with only a few actuators applied inside; individual joint torque does not need to be specified a preset value, which reduces the difficulty of control. In addition to the HIT/DLR II mentioned above, the other famous UA hands such as the 15-DOF Laval hand,¹² the SDM hand,¹³ and the multifunctional anthropomorphic prosthetic hands are all very representative.^{14,15}

In the prior researches on UA hand structures, Birglen and Gosselin¹⁶ present a three-phalanx UA finger combining linkage mechanism and spring to achieve the self-adaptability, which allows it to adjust itself to irregularly shaped objects. While joint angles between each phalange keep fixed before the proximal phalange touches object, this is obviously not an anthropomorphic way like human. In order to realize the coupled and self-adaptive movement, Li et al.¹⁷ present a two-phalanx finger based on pulley and gear, which can realize coupled anthropomorphic, self-adaptive motion and achieve experimental verification, while the number of the components is up to 16 except the motor in total. Besides the complex structure, the finger can just achieve its own self-adaptability, which means each finger needs to be driven independently to realize the whole hand self-adaptability. The novel UA finger structure proposed in this article is based on Birglen's research, combining the linkage mechanism and spring, which can realize coupled, self-adaptive motion as the UA finger proposed by Li, while only six components are included. Moreover, an UA transmission mechanism is proposed to connect the independent finger, which makes each connected fingers work in a cooperative way. Therefore, the self-adaptability promotes from an independent finger to the whole hand without increasing the number of actuators. The feature of the proposed hand is similar to Gosselin's work; however, there are some shortage in tendon-driven mechanism relative to linkage mechanism in practical application,

which will be described later. Moreover, in addition to the ability that allows the hand to adjust itself to an irregularly shaped object without complex control strategy and sensors,¹⁶ the grasping stability should also be taken into consideration. This article innovatively puts forward a method of obtaining the grasping stability through calculating the contact force; thus, the range of the grasping static equilibrium is obtained.

This article is organized as follows: section "Design of UA hand" presents the UA transmission mechanism of hand in detail first and then summarizes the grasping process. Section "Force analysis of the UA finger" analyzes the fingers' grasping forces in different grasp modes. Section "Stability analysis of UA hand" analyzes the grasping stability of the UA hand and shows the range of the static equilibrium. Grasping experiments are illustrated in section "Experiments of the UA hand," followed by conclusions in section "Conclusion."

Design of UA hand

In this section, the structure of UA finger is presented first. Then, the grasping process analysis of the single finger and the cooperative fingers will be given.

Structure of UA finger

For an anthropomorphic hand, in addition to owning to many functions, the finger mechanism must be very compact to preserve the overall size. A healthy person's finger is composed of three phalanges connected with three joints, the metacarpophalangeal (MCP) joint, the proximal interphalangeal (PIP) joint, and the distal interphalangeal (DIP) joint. To compromise the versatility and simplicity, the UA finger proposed in this article only has the MCP joint as the PIP joint, and the DIP joint's motion is negligible relative to the PIP joint, only about 50% of the PIP joint's;¹⁸ therefore, the proposed UA finger only contains the proximal phalange and the distal phalange.

Tendon-driven mechanism is widely used in the UA finger mechanism due to its flexibility and simple structure, such as the Shadow Hand and Gosselin's pioneering work; however, it can only exert small grasping force which is unable to do heavy work. The other disadvantage of tendon systems is that they are strongly affected by friction and elasticity.^{19,20} Therefore, a linkage mechanism with springs for a finger mechanism was proposed by Licheng and Ceccarelli²¹ and Shuangji et al.²² As linkage mechanism consists of rigid links and transmission gears, it is more convenient for applications where large grasping forces are required, and the finger and hand kinematics can be easily modeled and solved as a standard kinematics problem for control purposes.²³

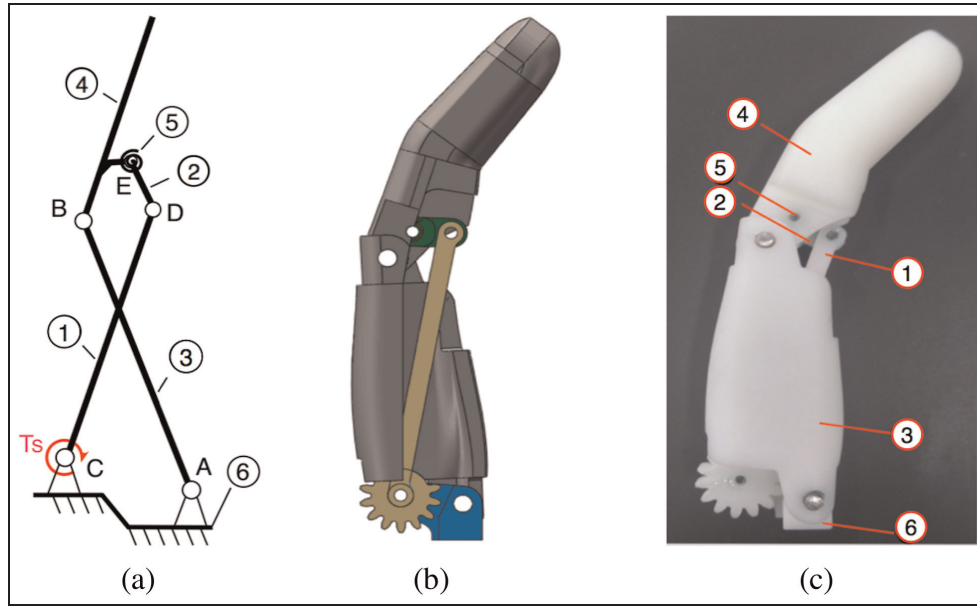


Figure 1. (a) Schematic diagram of the UA finger, (b) 3D model of it, and (c) its prototype produced by 3D printer with ABS material. The main parts are presented in (a) and (c).

①: Link_1; ②: Link_2; ③: proximal phalange; ④: distal phalange; ⑤: spring_1; ⑥: base.

Figure 1 shows the schematic diagram of the UA mechanism the 3D model of the UA finger and its prototype produced by three-dimensional (3D) printer. The novel UA finger mainly consists of four bars, a base, and a torsion spring. A and B represent the MCP joint and PIP joint, respectively, and C, D, and E represent the other revolute joints of the linkage mechanism, and the torsion spring is located at point E connecting the distal phalange and Link_2. Motor is embedded in the palm with a gear connection at joint C; the torque T_s is transmitted from the motor to rotate Link_1. As the two phalanges' motion transmission is connected with the linkage mechanism with spring, the finger can realize coupled motion and self-adaptive motion; the grasping process will be introduced in detail later.

Grasping process of UA hand. The grasping process of the UA hand is divided into two parts, the individual grasping process of one UA finger and the cooperative grasping process of the two fingers. The grasping process of one UA finger is shown in Figure 2, where the grasping process is simulated through the 3D model of the finger. The process consists of two sequential modes: coupled grasp mode and self-adaptive grasp mode. Figure 2(a) shows the initial state of the finger that all the phalanges are maintaining at the relaxed state like human. When the finger starts grasping work, the motor drives Link_1 to rotate through the gear transmission. Before the proximal phalange contacts the object as shown in Figure 2(b), the finger works at coupled grasp mode. During the coupled grasp mode, the torsion spring keeps its initial state without any deformation, which constrains

Link_2 and the distal phalange to be connected fixedly, namely, Link_2 will not rotate relative to the distal phalange at the joint E. When the finger works with the coupled grasp mode, the proximal phalange and distal phalange are assumed to be driven by the four-bar linkage ABCD marked in red line.

Once the proximal phalange touches the object tightly as shown in Figure 2(b), it cannot rotate any more, namely, the contact point F is assumed to be fixed on the base. In the case that the proximal phalange collides with the object while the distal phalange is still free, the UA finger turns into the self-adaptive grasp mode. In this mode, under the action of torque from motor on Link_2 and the reaction force exerted from the object on the proximal phalange, the torsion spring starts to deform. Thus, rotation of motor can still be transmitted to Link_1 through the four-bar linkage DBEC marked in red line as shown in Figure 2(b). Even though the rotation of the proximal phalange is constrained, the distal phalange can still rotate until it touches the object as well. This four-bar linkage DBEC could meet singularity when segments BE and CE are collinear, where Link_1 cannot drive the distal phalange to rotate relative to the PIP joint anymore, this is the mechanical limitation for the UA finger, while with the force exerted from the torsion spring, the distal phalange will extend when the torque acting on Link_1 from the motor is released. As shown in Figure 2(c), the self-adaptive grasp is achieved.

The self-adaptive movement above is merely for a single finger; in order to further enhance the self-adaptability of the dexterous hand, this article puts

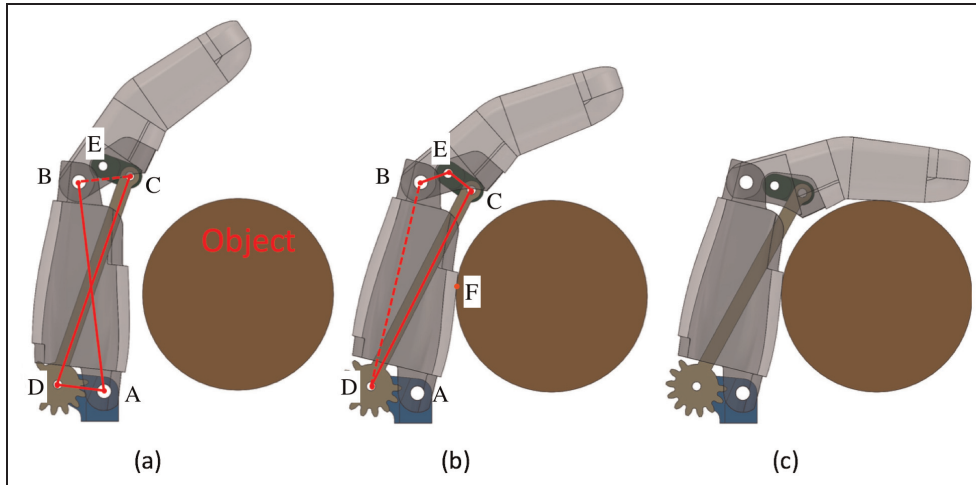


Figure 2. (a) Coupled grasp mode, (b) self-adaptive grasp mode, and (c) self-adaptive grasp achieved.

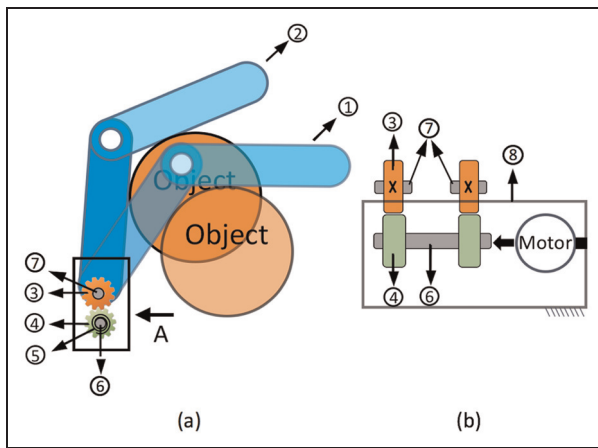


Figure 3. (a) Cooperative grasping process and (b) schematic diagram of the transmission mechanism. The main parts are presented in (a) and (b).

①: front finger; ②: hinder finger; ③: gear_1; ④: gear_2; ⑤: spring_2; ⑥: motor shaft; ⑦: finger shaft; ⑧: palm.

forward a cooperative transmission mechanism that connects the independent UA fingers to a UA hand. Figure 3 shows the schematic diagram of the cooperative transmission mechanism for two UA fingers and the cooperative grasping process of them. The gear_1 is fixedly sleeved on the finger shaft and fixedly connected with Link_1. The gear_2 is rotatably sleeved on the motor shaft. The key part of the mechanism is the torsion spring_2 that connects gear_2 and the motor shaft for both the two fingers, whose stiffness is larger than that of torsion spring_1 embedded in the finger, as shown in Figure 3(b). When the grasp starts, the motor fixed on the palm drives the motor shaft to rotate. As shown in Figure 3(a), before the two fingers touch the object, the motor shaft is assumed to be fixed with gear_2 due to the connected spring_2 and drives the

fingers both working in coupled grasp mode. When the hinder finger's proximal phalange collides with the object, spring_1 of the hinder finger starts deforming first and the hinder finger enters its self-adaptive grasp. After the self-adaptive grasp of the hinder finger is achieved, spring_2 that connects the hinder finger and the motor shaft starts deforming; thus, though the hinder finger is blocked by the object, the motor can still rotate to drive the front finger rotating until its self-adaptive grasp is achieved. Moreover, this protects the motor from being damaged when a sudden impact is acted on the fingers.

The analysis above shows the grasping process of the proposed mechanism. With the cooperative transmission mechanism and the UA finger, the UA hand can not only ensure the anthropomorphism of the grasping process but also be capable to encompass objects of various shapes and sizes, such as a cone. Therefore, this UA hand is able to be applied as an effective end-effector in the unstructured environments.

Force analysis of the UA finger

To achieve an effective grasping, the grasping forces of the phalanges should be large enough to maintain the object grasped stably. Different finger grasping force modes due to the UA characteristic is first presented in the section. In the end of this section, the grasping force of the whole 2-joint UA finger is analyzed in detail, which will be used in the grasping stability analysis.

Classification of grasp mode

As the UA finger has the selfadaptability to grasping object according to its size and shape, which leads the grasping force model to be quite different. Grasping force models of the 2-joint UA finger can be divided into two categories according to the number of the

contact points: the entire grasp mode and the fingertip grasp mode. For the entire grasp mode, when the proximal phalange touches the object earlier than the distal phalange, the distal phalange will keep rotating until it touches the object as well. However, this ideal grasping sequence might not always occur, if the distal phalange touches the object earlier than the proximal phalange; therefore, the finger works in the fingertip grasp mode. In the entire grasp mode, both phalanges offer grasping forces on object, while in the fingertip grasp mode, only the distal phalange offers grasping force on object, so the fingertip grasp mode is not quite stable as the entire grasp mode because of the lack of grasping force from the proximal phalange.¹⁷ When analyzing the grasping force of a finger, only contact pressure is considered and the contact friction is ignored. Therefore, the contact force defined in this article is perpendicular to the phalange contact surface. In addition, only positive contact force is considered to be feasible when the finger achieves an effective grasp; if a negative contact force occurs, the corresponding phalange will separate from the object. In the entire grasp mode, the grasping forces F_1 and F_2 are both positive, while in the fingertip grasp mode, the contact force F_1 equals to zero, which means the proximal phalange contact is lost.

Grasping force analysis

Detailed force analysis will be presented in this section. Figure 4 shows the grasping force model when the UA finger has grasped an object in the entire grasp mode. Although the actual forces exerted on the phalanges are not exactly the same as the diagram, it has the same effect. In the schematic diagram, the proximal phalange length L_1 and the distal phalange length L_2 are

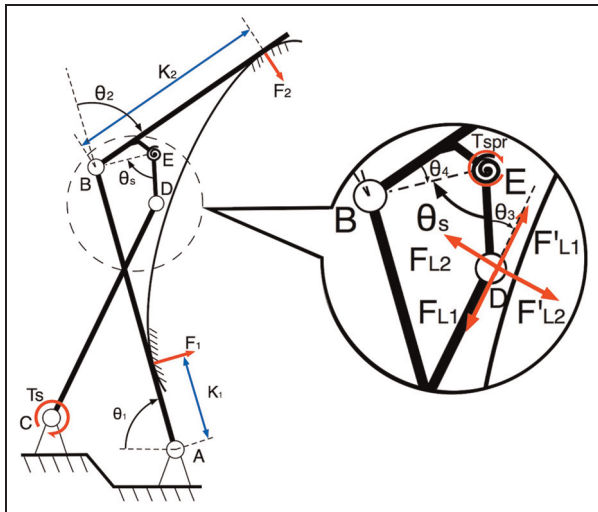


Figure 4. Grasping force model of the UA finger.

predesigned geometric parameters; F_1 and F_2 are, respectively, the normal contact forces acting on the proximal phalange and the distal phalange; K_1 and K_2 are, respectively, the contact locations on their respective phalanges; θ_1 and θ_2 are the joint angles for the MCP joint and the PIP joint, respectively; and θ_s is the deformable angle of the torsion spring.

In order to determine the magnitude of the contact forces that the UA finger can apply to the object, a quasi-static model was developed,^{16,24} and the following expressions were obtained as equation (1)

$$\begin{cases} F_1 = \left[\frac{K_2(1+R) + RL_1 \cos \theta_2}{K_1 K_2} \right] T_s \\ F_2 = \frac{RT_s}{K_2} \end{cases} \quad (1)$$

where F_1 , F_2 , K_1 , K_2 , T_s , T_{spr} , and θ_2 are the parameters depicted in Figure 4, and R is the transmission relationship characterizing the mechanism used to transmit the actuation torque T_s to the torque on the PIP joint. This factor depends on the stable state of the fingers, namely, the current joint angles, θ_1 and θ_2 . The values of F_1 and F_2 can be achieved by analyzing the state shown in the detail view in Figure 4.

First of all, Link_1 is torque balanced with respect to joint C under the effect of the torque T_s , and forces F_{L1} and F_{L2} are the forces exerted on Link_1 and Link_2, respectively. Second, Link_2 is torque balanced with respect to joint C under the effect of F'_{L1} , F'_{L2} , and the torque T_s . As F_{L1} and F'_{L1} and F_{L2} and F'_{L2} are two pairs of interaction forces, $F_{L1} = F'_{L1}$ and $F_{L2} = F'_{L2}$. Therefore, the transmission external forces F_{L1} and F_{L2} from the T_s through joint B can be achieved as equation (2)

$$\begin{cases} F_{L1} = \frac{T_{spr} + \cos \theta_3 L_{DE} F_{L2}}{\sin \theta_3 L_{DE}} \\ F_{L2} = \frac{T_s}{L_1} \end{cases} \quad (2)$$

where θ_3 is constrained by θ_1 and θ_2 .

At the same time, torque on the distal phalange with respect to the PIP joint B is balanced under the effect of F'_{L1} , F'_{L2} , and F_2 . The contact force F_2 is achieved through the torque balance equation and expressed as equation (3)

$$F_2 = \frac{\cos(-\frac{\theta_s}{2} + \theta_3) F'_{L1} - \sin(\frac{\theta_s}{2} + \theta_3) F'_{L2}}{K_2} L_{BD} \quad (3)$$

Finally, the torque on proximal phalange is balanced with respect to the MCP joint under the effect of F_1 , F_2 , F'_{L1} , and F'_{L2} . Thus, expression of F_1 in the entire grasp mode can be expressed as equation (4)

$$F_1 = \frac{\cos \theta_2 F_2 + \sin \theta_{sum} F'_{L1} + \cos \theta_{sum} F'_{L2}}{K_1} L_1 \quad (4)$$

Table 1. Mechanical parameters in force analysis.

Label	Parameters
L_{BE}	6 mm
L_{DE}	6 mm
K_1	30 mm
K_2	14 mm
k_{spr}	0.3 Nm/°
k_s	6.5 Nm/°
z_1	14
z_2	14

where $\theta_{sum} = \theta_2 + \theta_3 + \theta_4 - \theta_s$.

All of the gravity of the finger is ignored in the analysis as the phalanges' weights are too small compared with the grasping forces. Assume that when the proximal phalange touches the object, the length of the virtual link BD is L_{BD0} , and the angle of θ_T is θ_{T0} , and when the distal phalange continues rotating until the entire grasp mode is achieved, the final angle of θ_T turns into θ_{Tf} , and the length of BD turns into L_{BDf} . The relationship between L_{BD} and θ_T is one-to-one correspondence, and the deformable angle of the torsion spring θ_s can be expressed according to L_{BD}

$$\theta_s = a \cos \left(\frac{L_{BE}^2 + L_{DE}^2 - L_{BDf}^2}{2L_{DE}L_{BE}} \right) - a \cos \left(\frac{L_{BE}^2 + L_{DE}^2 - L_{BDi}^2}{2L_{DE}L_{BE}} \right) \quad (5)$$

The torsion spring embedded in the finger is ideal which satisfies Hook's law, so is the torsion spring which connects motor shaft and gear_2 in Figure 3, and the following relationship can be expressed as

$$\begin{cases} T_{spr} = k_{spr}\theta_s \\ T_s = \frac{z_1}{z_2}k_s\Delta\theta_M \end{cases} \quad (6)$$

where z_1 and z_2 are the numbers of teeth of gear_1 and gear_2, respectively; k_{spr} and k_s are the elasticity coefficients of the torsion springs; and $\Delta\theta_M$ is the extra rotation angle of the motor shaft relative gear_2.

Substituting equation (6) into equations (3) and (4), the grasping force of the finger can be obtained. In order to show the relationship between the contact forces of each phalange and the joint angles of each joint, some required parameters are designed and shown in Table 1. The relationships between the grasping forces and the rotation angles of joints based on the actual finger mechanism are depicted in Figure 5.

As depicted in Figure 5(a) and (b), the maximum contact force of the proximal phalange F_1 is about 43.5 N, and the maximum contact force of the distal phalange F_2 is about 11.9 N. When θ_1 increases, the value of F_1 decreases, and when θ_2 increases, the value

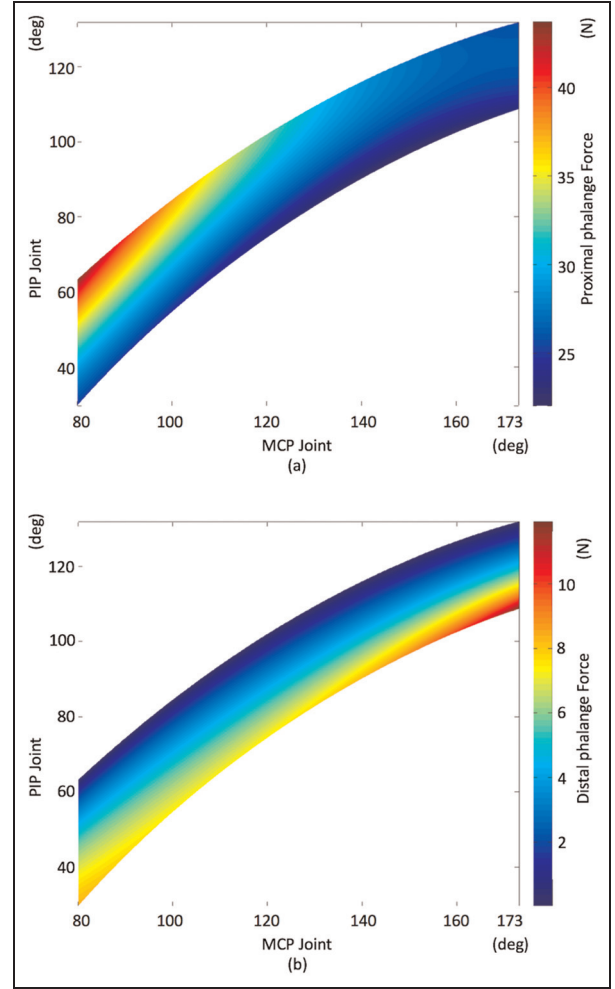


Figure 5. (a) Value of the contact force F_1 relative to the angles of the MCP joint and the PIP joint and (b) value of the contact force F_2 relative to the angles of the MCP joint and the PIP joint.

of F_1 increases. While the case for F_2 is opposite, when θ_1 increases, the value of F_2 increases, and when θ_2 increases, the value of F_2 decreases. This is because the output torque T_s to Link_1 from the motor is constant, while the two phalanges share this torque through the UA finger transmission system, so the two contact forces of the phalanges in the grasping process present a complementary characteristic.

For the fingertip grasp mode, only the distal phalange touches the object. The force on the distal phalange relative to the joint angles is same as the analysis of the entire grasp mode. The difference is that the proximal phalange reaches its mechanical limitation so the contact force on the proximal phalange F_1 is a constant value of 0 N.

Stability analysis of UA hand

The performance of an UA hand is mainly determined by its mechanical design and to a lesser extent by the

control of the hand.²⁵ The most critical criterion is the grasping stability, in this article it means the range of the rotation of the hand, during which the object is force balanced by the fingers and palm. Grasping stability is constrained by many conditions, including the size, shape, weight of the object, and the posture and contact forces of the UA hand during grasp. In the first half of the section, the objective is to analyze the constraints caused by the parameters of the object in successful stable grasp, such as the size, shape, weight. In the second half of the section, the effect of the posture will be presented, and the grasping stability will also be analyzed.

Grasping range analysis

Due to the UA characteristics of the hand, the hand is able to self-adapt to objects of various shapes and sizes. As the shape of various objects does not have a uniform definition and cannot be calculated reproducibly, for simplicity, all the referred objects' shape analyzed in this article are supposed to be cylindrical, whose size is characterized by its radius r_{obj} . As the two cooperative fingers complete the same action while grasping a cylindrical object, a grasping hand can be projected onto a plane made up of the index finger, the thumb, and the palm. Thus, the UA hand grasping model is simplified to a two-dimensional (2D) model on a plane.

The range of object sizes which can be grasped by an UA hand depends on the UA finger's geometric parameters. Due to the symmetry of the mechanism between the index finger and the thumb, the grasped objects keep symmetry relative to them when the palm keeps vertical upward. According to r_{obj} of the object, a 2D hand consists of two fingers with two phalanges, and a palm can grasp cylindrical objects with 5, 4, 3, or 2 contact points.²⁶ Based on Cutkosky's taxonomy,²⁷ the proposed UA hand can reproduce more than 80% grasping behaviors of the human hand presented by Cutkosky (6/9 of the power grasp and 7/7 of the precision grasp, the medium wrap, adducted thumb, and light tool are excluded due to the fact that the thumb cannot rotate relative to the palm). As this article focuses on the stability analysis of the grasp, thus a power grasp is more suitable than precision grasp. A five-point grasp is most preferred because the object is enveloped with all phalanges and the palm, namely, each finger is in entire grasp mode as mentioned in last section, and the palm can also provide contact force to keep the object stable. Thus, a five-point grasp is consisted of two entire grasp finger-object model and an object-palm contact model, as depicted in Figure 6, and its grasping stability will be analyzed in the second half.

When the object is entirely grasped by the UA hand, the size of the object is determined by the contact points; in addition, in order to ensure that this is a

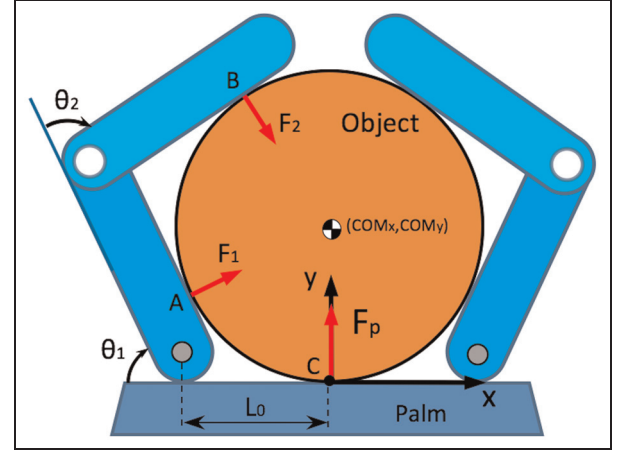


Figure 6. The five-point grasping model: A, B, and C are the contact points of the object with the phalanges and the palm; F_1 , F_2 , and F_p are the contact forces, respectively; and COM_x and COM_y represent the coordinates of the object.

stable grasping, some constraints must be met. For a five-point grasp, as the object contacts with the palm and phalanges, COM_y equals to the radius of the object r_{obj} ; in addition, as the shape of the object is cylindrical, the constraints $K_1 = L_0$ and $K_2 = L_1 - K_2$ should be satisfied. However, the constraints above can only guarantee that the object is five-point grasped; to ensure that the object is entirely enveloped by the hand with a stable grasp, constraints of the hand gestures and contact forces must be satisfied as well.

The hand gesture can be defined with loop closure vector equations between the object and the phalanges with respect to MCP joint, and the equations are expressed as follows, so are those of the symmetric finger

$$\begin{pmatrix} L_0 + \cos \theta_1 K_1 \\ \sin \theta_1 K_1 \end{pmatrix} = \begin{pmatrix} \sin \theta_1 r_{obj} \\ COM_y - \cos \theta_1 r_{obj} \end{pmatrix} \quad (7)$$

$$\begin{pmatrix} L_0 + \cos \theta_1 L_1 + \cos(\theta_1 + \theta_2) K_2 \\ \sin \theta_1 L_1 + \sin(\theta_1 + \theta_2) K_2 \end{pmatrix} = \begin{pmatrix} \sin(\theta_1 + \theta_2) r_{obj} \\ COM_y - \cos(\theta_1 + \theta_2) r_{obj} \end{pmatrix} \quad (8)$$

where K_1 , K_2 , θ_1 , θ_2 , and L_1 have same definition as before. (COM_x, COM_y) is the coordinate of the center of the object relative to the coordinate C, whose origin locates at the contact point between the object and the palm, and x-axis is parallel to the palm. L_0 is the distance between the contact origin C and the MCP joint. Equation (7) is based on the coordinate of the contact point B, and equation (8) is based on the coordinate of the contact point C.

This article gives a special case that the hand keeps vertical upward first, and the gestures and the contact

forces of the index finger and the thumb are symmetrical. Therefore, the objects are enveloped only if the rotation angles of the phalanges satisfy the following inequality: $\theta_1 + \theta_2 \geq \pi/2$. The values of θ_1 and θ_2 can be calculated by combining equations (7) and (8), and the result is expressed as follows

$$\begin{cases} \cos \theta_1 = \frac{r_{obj}^2 - L_0^2}{r_{obj}^2 + L_0^2} \\ \cos \theta_2 = \frac{r_{obj}^2 - (L_1 - L_0)^2}{r_{obj}^2 + (L_1 - L_0)^2} \end{cases} \quad (9)$$

Substituting $\theta_1 + \theta_2 = \pi/2$ into equation (9), the maximum object size r_{obj_max} that can be enveloped with five-point grasp is obtained as

$$r_{obj} \leq \frac{1}{2} \left(L_1 + \sqrt{L_1^2 - 4L_0^2 + 4L_1L_0} \right) \quad (10)$$

All the objects whose r_{obj} is smaller than the $r_{obj_max} = 45$ mm can be entirely enveloped only if the joint angles are included in the finger motion workspace. The r_{obj_min} is limited to 32 mm by solving the finger motion workspace with numerical analysis.

To achieve a quasi-static state of the five-point grasp, the object should be balanced under its gravity and the contact forces of the phalanges and the palm as shown in Figure 6. The contact forces of the phalanges have been analyzed in section “Force analysis of the UA finger,” and its relationship between its values of the joint angles is shown in Figure 5. The contact force of palm is always vertical to the palm as shown in Figure 6. When the object is against the palm, the contact force with the palm must be positive. When the contact force with the palm equals to zero, the hand is in the critical state of four-point grasp and five-point grasp. Obviously, in the case that the object mass is constant, the greater the contact force with the palm, the more stable the grasp. The relationship between the contact force of the palm and the parameters of the object, including the mass and r_{obj} , is shown in Figure 7.

In a five-point grasping, the rotation angles of the joints θ_1 and θ_2 and the positions of the contact points K_1 and K_2 are fully determined by r_{obj} ; this was shown in section “Grasping range analysis.” Moreover, the values of the contact forces of the palm depend on r_{obj} as well.

As shown in Figure 7, when the object gravity is constant, the smaller the r_{obj} is, the more tightly the object be pushed against the palm, which means larger contact force with the palm. The blue curve divides the contact force region according to its value, and the value of the contact force under the line is below zero, which means that the five-point grasping cannot be achieved. In other words, to achieve a stable five-point grasping, the object must satisfy a certain mass for a specific r_{obj} .

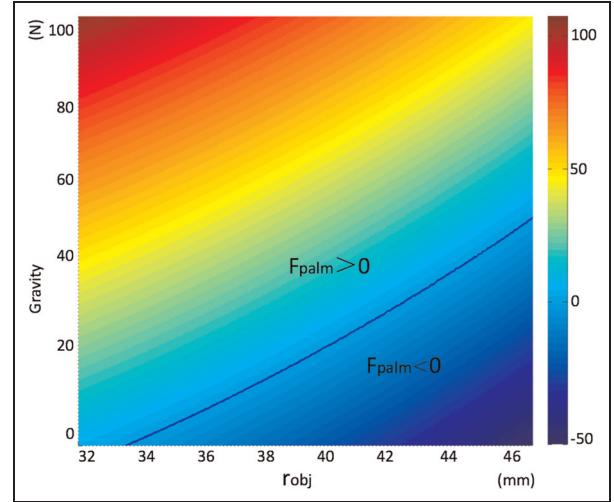


Figure 7. The relationship between the contact force of the palm relative to the gravity and the radius of the object, and the blue curve is the boundary where the contact force equals to 0 N.

The case talked above is just the special one where the hand is keeping a vertical upward gesture. However, for a common situation of grasp, the gesture of the hand is not always remaining invariant. Therefore, the rotation of the hand in the 2D plane will be analyzed in this article to imitate the rotation of the wrist. This gesture change makes the gravity of the object not perpendicular to the palm, which will lead the component of the gravity in the y -direction to decreasing, while the component in the x -direction is not still zero; therefore, the symmetry between the index finger and the thumb is broken, so is the original static equilibrium. In order to maintain the five-point grasping state, the object will slide along the x -direction to achieve a new static equilibrium state under the contact forces.

With the inclination of the hand, the object will generate a motion of sliding relative to the palm under the effect of the gravity. As the contact forces cannot guarantee the static equilibrium of the object, the fingers will also change their gestures, namely, the joint angles, the contact points, and the contact forces between the fingers and the object are changed according to the change in the joint angles, which is analyzed in section “Grasping force analysis.” In this process, as the rotation speed of hand is very slow, the acceleration of the object caused by the contact forces and gravity is neglected; therefore, the entire process from imbalance to the static equilibrium is considered to be quasi-static.

The object will eventually remain in three kinds of states: the first is the ideal one that the object maintains in a new static equilibrium under the contact forces and gravity; meanwhile, the five-point grasping is maintained. In the second case, the object can also maintain in static equilibrium under the contact forces and gravity,

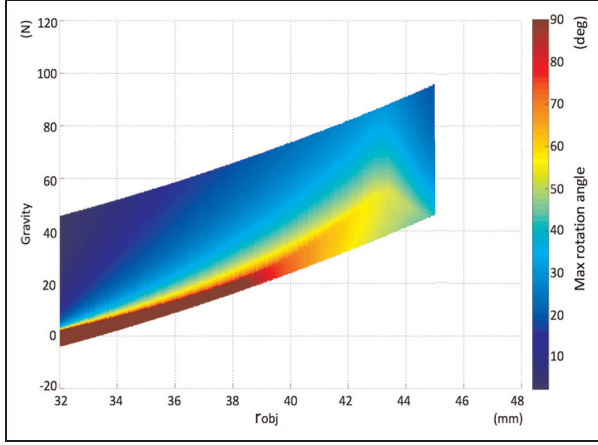


Figure 8. The stable rotation range of the equilibrium state relative to the gravity and the radius of the object.

while some contact forces with palm or phalanges equal to zero, which means that some contact points are lost and the object is not still in a five-point grasping state but in other state mentioned above. The third case is a complete failure, where the finger moves from initial symmetrical position to its limitation, while the contact forces are not able to balance the component of the gravity in the x -direction; finally, the object slip out of the hand. The latter two cases are considered to be failed in this article, and the other grasp equilibrium states in the second case will be analyzed in the future research.

For the successful case, the object will slide on the palm plane with the inclination of the hand, the gestures of the fingers change, their joint angles can be obtained by solving equation (9), and the contact forces between them and the object can be calculated according to equations (3) and (4). In the case of satisfying the contact force with the palm is above zero, the object will keep sliding until the contact forces balance the gravity.

Figure 8 shows the available rotation range of the hand with object of various weights and r_{obj} in hand, that is, when the object is defined with certain radius and mass, the rotation range of the hand maintains in the equilibrium state. The weight of the object with defined r_{obj} is constrained to be 5 kg heavier above the basic blue curve in Figure 7. Figure 8 depicts the boundary of the stable grasp; when the hand is in the vertical state, all the objects range from r_{obj_min} to r_{obj_mix} with certain mass to maintain in the equilibrium state. With the rotation of the hand, the equilibrium state of the object cannot be maintained when rotating to a particular value, that is the equilibrium boundary, and the equilibrium states between the boundaries are continuous. Figure 8 shows the range of the equilibrium state relative to the parameters of the object clearly. As shown in Figure 8, the object with lower weight has higher range of the equilibrium state, when the weight increases, the range decreases. However, when r_{obj}

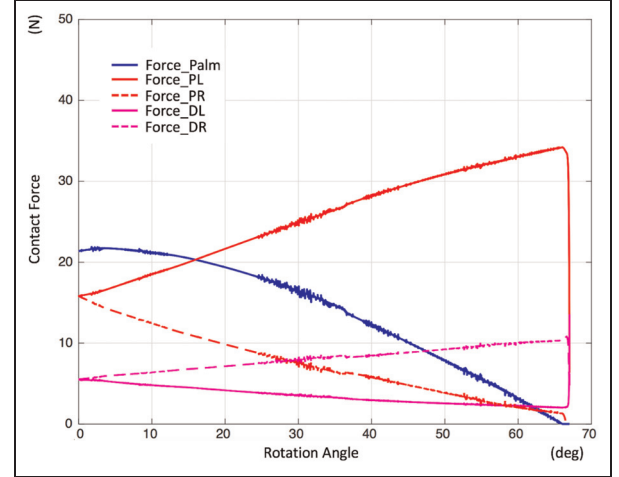


Figure 9. Simulation result of the hand rotation, the object is 38 mm radius and 2.43 kg weight, the y-axis represents the contact force of the phalanges and the palm, the x-axis represents the rotation angle of the hand from right to left, the blue curve represents the contact force of the palm, the red and pink solid lines represent the contact forces of the left finger's proximal and distal phalanges, and the dashed lines represent those of the right finger.

increases, the range increases before r_{obj} reaches 43.2 mm, and when r_{obj} increases from 43.2 mm, the range starts to decrease.

A simulation is done to simulate the hand rotation in ADAMS, where r_{obj} is 38 mm, the weight is 2.43 kg, and the rotation is from the right to the left. Figure 9 shows the curves of the contact forces; the indices “P” and “D” mean the proximal phalange and the distal phalange, respectively, and the indices “L” and “R” mean the left finger and the right finger, respectively. As shown in the curves, the contact forces of the distal phalanges are both very small compared with those of the proximal phalanges as depicted in Figure 5, as they are playing the role of guarantee that objects do not slide off. The contact force of the left proximal phalange is increasing to balance the component of the gravity, while the contact force with the palm is decreasing with the rotation of the hand and equals to zero when this rotates to about 65° where the object slides off the hand. The calculated value of the is 63.5°, which is very close to the simulation result, and the error is due to that in the simulation the hand is rotating in a low-speed condition instead of in an absolutely static condition in the force analysis.

Experiments of the UA hand

Figure 10 shows the self-adaptability of a single finger and the grasp ability of the whole hand. Figure 10(a)–(c) shows the self-adaptability of a single finger to objects of various sizes and shapes, such as ball,

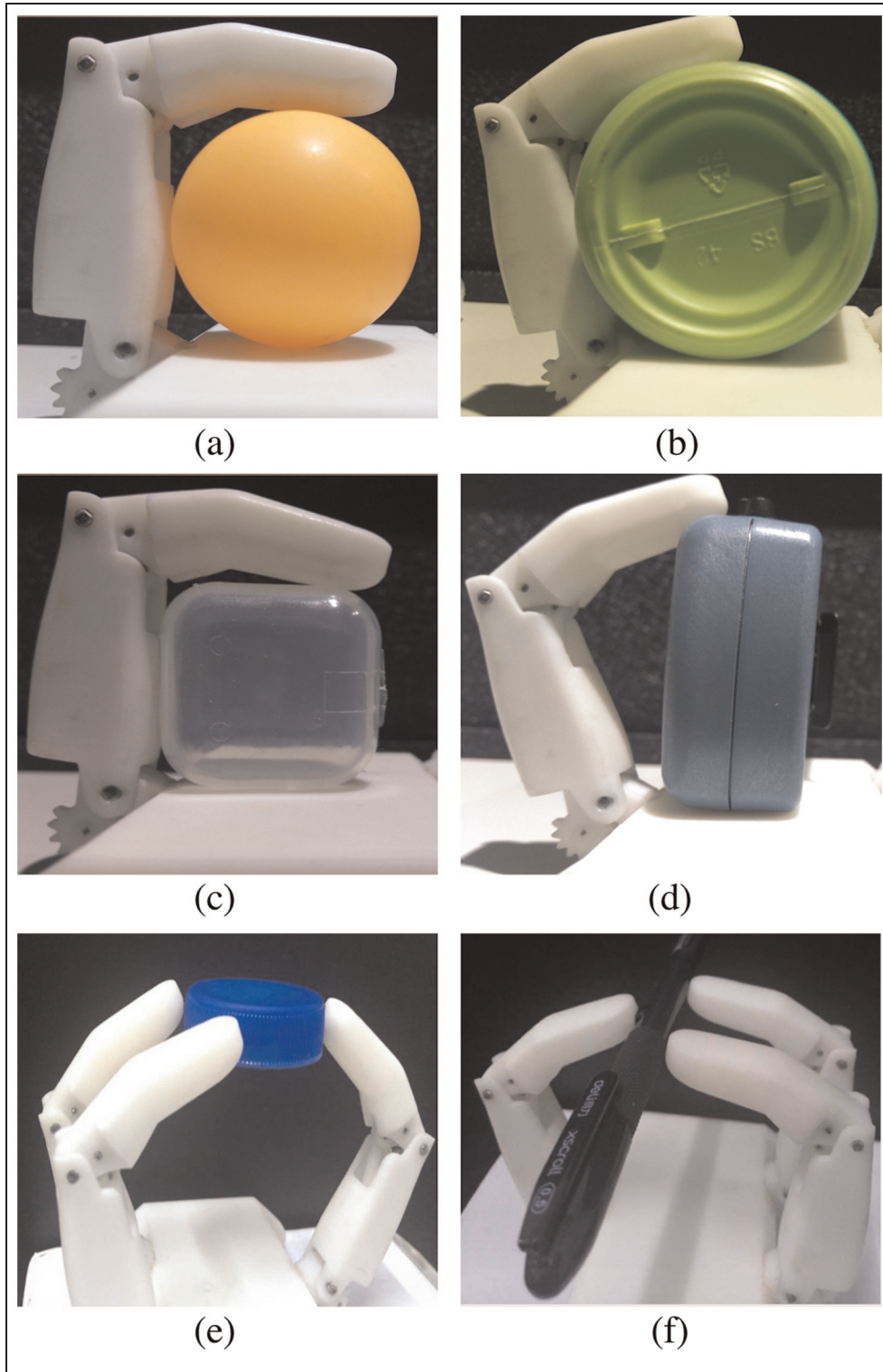


Figure 10. Prototype of the UA hand and its grasping process: (a)(c) entire grasp mode for objects of various sizes and shapes, (d) fingertip grasp mode, and (e)(f) precision grasp.

cylinder, and cuboid. It is obviously seen that all the objects can be entirely involved by the finger. Figure 10(d) shows the finger working in fingertip grasp mode when grasp is an irregular object. Figure 10(e) and (f)

verifies the ability of precision grasping objects of various sizes and shapes presented in Cutkosky's taxonomy.

Figure 11 shows a complete grasping motion process of the cooperative fingers driven by one motor. In

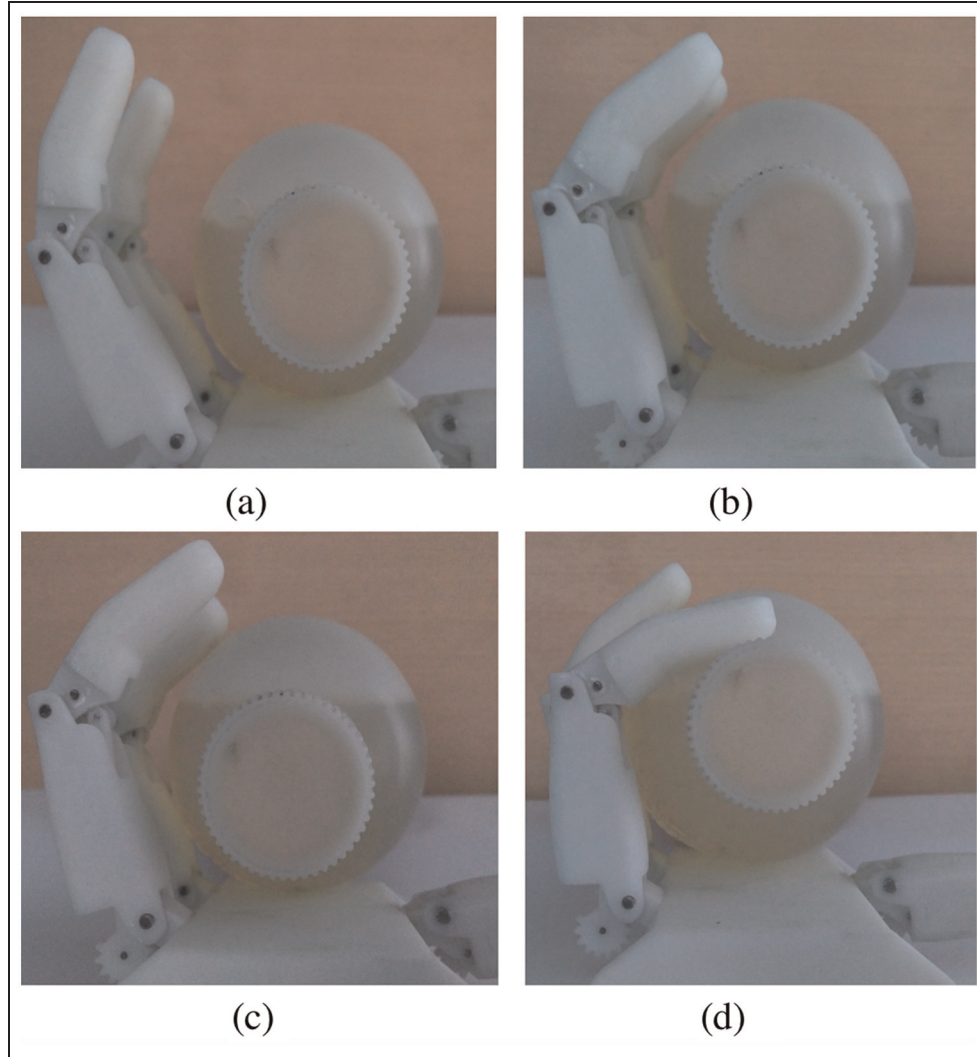


Figure 11. Prototype of the UA hand and its grasping process: (a)(b) coupled mode for the hinder finger and the front finger and (c)(d) self-adaptive mode for the front finger.

Figure 11(a), when both the cooperative fingers have not touched the objects, each of their movements is in the coupled grasp mode, and the relationship between the proximal phalanges and the distal phalanges follows the coupled mode; when the hinder finger's proximal touches the object, its working process mode turns to the self-adaptive mode, and its distal phalange can continue rotating until it touches the object, as shown in Figure 11(c). Due to the cooperative transmission mechanism, the front finger's movement is independent of the hinder finger's, as shown in Figure 11(b) and (c), when the hinder finger achieves its entire grasping mode and blocked by the object, the front finger is still working in the coupled mode all the time until the front finger achieves its fingertip grasp mode (Figure 11(d)).

The experiment of the UA hand grasping stability is shown in Figure 12; a cylindrical bottle with radius of 42mm and quality of 3.42 kg is five-point grasped by

the hand. In Figure 12(a), the palm is in the state of vertical upward, where the thumb and cooperative fingers keep symmetry, and the contact point with the palm is located at the center of the palm. By rotating the base of the UA hand, the static equilibrium is broken, the bottle starts sliding relative to the palm, and the corresponding changes in the fingers' postures have also taken place, and the joints' angles have changed to adjust the contact forces to balance the component of the gravity, as shown in Figure 12(b)–(d), which verified the stability analysis in section “Stability analysis of UA hand.”

Conclusion

In this article, a novel UA hand mechanism is designed and analyzed. The hand can realize human-like operations such as coupled motion and self-adaptive motion.

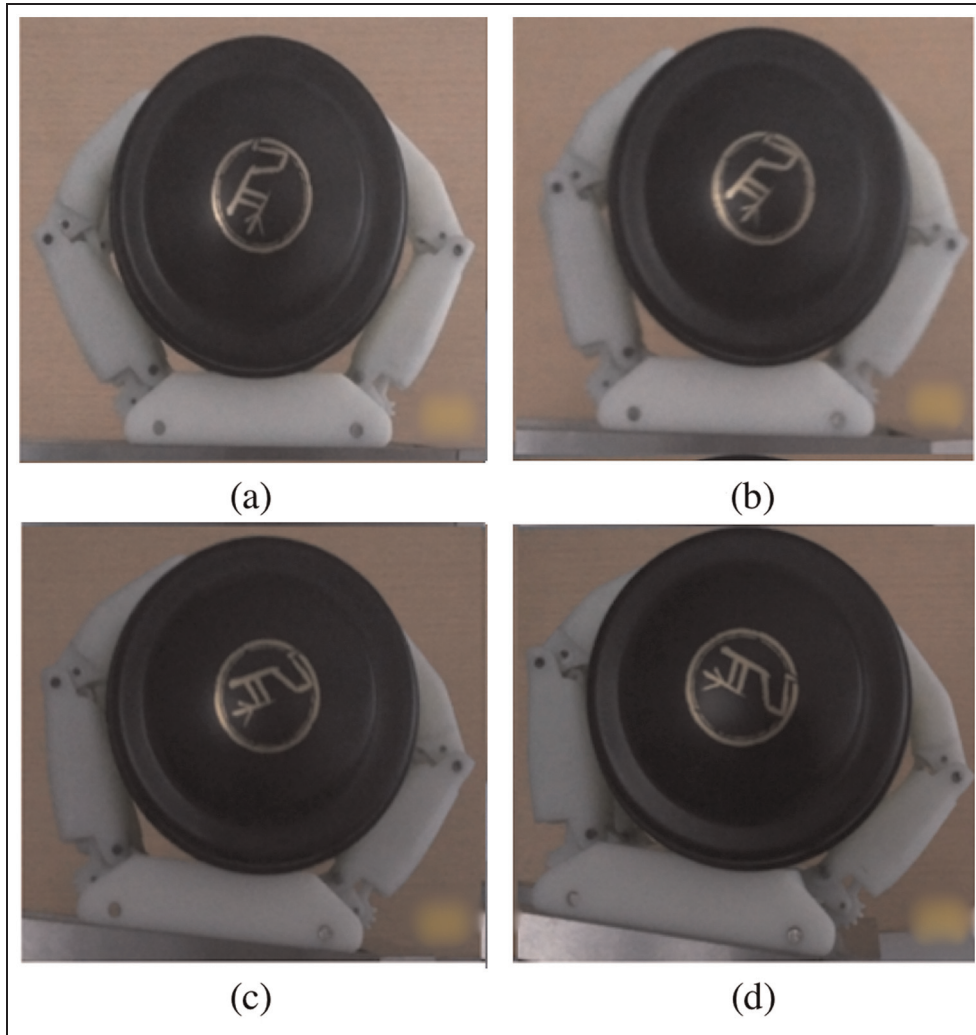


Figure 12. Experiment of the grasp stability: (a) the palm is vertical upward and (b)–(d) the static equilibrium during the rotating process of the hand.

Compared with belt-driven mechanism, the linkage mechanism has simpler structure, while compared with tendon-driven mechanism, the linkage mechanism has bigger grasping force and better controllability. The novel cooperative transmission mechanism promotes its self-adaptability to the entire hand. Grasping force analysis, grasping range analysis, and grasp stability analysis are discussed for the proposed UA hand. Finally, a series of experiments is done to verify the UA hand's grasping ability. The proposed hand adopts several UA mechanisms, which reduces the hand mass and size while preserving the ability of grasping objects of various sizes and shapes. This is very suitable for the prosthetic fields where accuracy and function requirements are not high, while hand mass and size are strictly limited. As a prosthetic limb end-effector, it could help upper limb amputee do some daily work, such as lifting a briefcase, holding a cup, opening a

door. However, the UA hand also has some limitations, such as the simplex mode, which makes it not able to achieve independent movement of multiple DOFs according to the control signals, such as the electromyography (EMG) signals. In addition, it cannot achieve the precise manipulation of the object so that it cannot help to do more complex daily work. Indeed, this article only makes a few steps for analyzing the grasp stability of the novel hand, and some constraints and conditions are simplified or ignored. The friction of the contact model is simplified, while for an accurate model, it is required. The contact model analyzed in this article only contains the power grasp, while for the precision grasp, whose contact points is less than the power grasp, is also very important especially for the precise operation. In the future work, these parameters will be taken into consideration to form a complete method for grasp stability analysis.

Authors note

Xuechao Chen is also affiliated to State key Laboratory of Robotics, Shenyang Institute of Automation, Chinese Academy of Sciences, Shenyang, China.

Declaration of conflicting interests

The author(s) declared no potential conflicts of interest with respect to the research, authorship, and/or publication of this article.

Funding

The author(s) disclosed receipt of the following financial support for the research, authorship, and/or publication of this article: This article was supported by the NSFC of China under grant nos 61533004, 61320106012, and 61673068; Beijing Municipal Science and Technology Project under grant no. D161100003016002; “111 Project” under grant no. B08043; and State key Laboratory of Robotics.

References

1. Mason MT and Salisbury JK. *Robot hands and the mechanics of manipulation*. Cambridge, MA: MIT Press, 1985, pp.879–880.
2. Jacobsen SC, Wood JE, Knutti DF, et al. The Utah/MIT dextrous hand: work in progress. *Int J Robot Res* 1984; 40: 423–442.
3. Bridgwater LB, Ihrke CA, Diftler MA, et al. The Robonaut 2 hand—designed to do work with tools. In: *IEEE international conference on robotics and automation*, Saint Paul, MN, 14–18 May 2012, pp.3425–3430. New York: IEEE.
4. Medynski C and Rattray B. Bebionic prosthetic design. In: *Proceedings of the 2011 MyoElectric controls/powerd prosthetics symposium fredericton*, 2011, <http://dukespace.lib.duke.edu/dspace/bitstream/handle/10161/4733/43%20Medynski.pdf?sequence=1>
5. Liu H, Wu K, Meusel P, et al. Multisensory five-finger dexterous hand: the DLR/HIT hand II. In: *IEEE/RSJ international conference on intelligent robots and systems*, Acropolis Convention Center, Nice, 22–26 September 2008, pp.3692–3697. New York: IEEE.
6. Rohling F, Haschke R, Steil JJ, et al. Platform portable anthropomorphic grasping with the Bielefeld 20-DOF shadow and 9-DOF TUM hand. In: *IEEE/RSJ international conference on intelligent robots and systems*, San Diego, CA, 29 October–2 November 2007, pp.2951–2956. New York: IEEE.
7. Bicchi A. Hand for dexterous manipulation and robust grasping: a difficult road toward simplicity. *IEEE Trans Robot Autom* 2000; 16: 652–662.
8. Bicchi A and Kumar V. Robotic grasping and contact: a review. In: *Proceedings of the IEEE international conference on robotics and automation*, San Francisco, CA, 24–28 April 2000, pp.348–353. New York: IEEE.
9. Baril M, Laliberte T, Gosselin C, et al. On the design of a mechanically programmable underactuated anthropomorphic prosthetic gripper. *J Mech Design* 2013; 135: 209–219.
10. Kragten GA and Herder JL. A platform for grasp performance assessment in compliant or underactuated hands. *J Mech Design* 2010; 132: 024502.
11. Birglen L, Laliberte T and Gosselin C. *Underactuated robotic hands*. Berlin, Heidelberg: Springer-Verlag, 2008, pp.171–207.
12. Gosselin C, Pelletier F and Lalibert T. An anthropomorphic underactuated robotic hand with 15 DOFs and a single actuator. In: *IEEE international conference on robotics and automation*, Pasadena, CA, 19–23 May 2008, pp.749–755. New York: IEEE.
13. Dollar AM and Howe RD. *The SDM hand: a highly adaptive compliant grasper for unstructured environments*, vol. 54. Berlin, Heidelberg: Springer, 2009, pp.3–11.
14. Dalley SA, Wiste TE, Withrow TJ, et al. Design of a multifunctional anthropomorphic prosthetic hand with extrinsic actuation. *IEEE/ASME T Mech* 2009; 14: 699–706.
15. Dalley SA, Wiste TE, Varol HA, et al. A multigrasp hand prosthesis for transradial amputees. *Conf Proc IEEE Eng Med Biol Soc* 2010; 2010: 5062–5065.
16. Birglen L and Gosselin CM. Geometric design of three-phalanx underactuated fingers. *J Mech Design* 2006; 128: 356–364.
17. Li G, Zhang C, Zhang W, et al. Coupled and self-adaptive under-actuated finger with a novel S-coupled and secondly self-adaptive mechanism. *J Mech Robot* 2014; 6: 678–683.
18. Chiri A, Giovacchini F, Vitiello N, et al. HANDEXOS: towards an exoskeleton device for the rehabilitation of the hand. In: *IEEE/RSJ international conference on intelligent robots and systems*, St. Louis, MO, 10–15 October 2009, pp.1106–1111. New York: IEEE.
19. Yong X, Jing X, Jiang Y, et al. Tendon drive finger mechanisms for an EMG prosthetic hand with two motors. In: *7th international conference on biomedical engineering and informatics*, Dalian, China, 14–16 October 2014, pp.568–572. New York: IEEE.
20. Carbone G. *Grasping in robotics*. London: Springer, 2013.
21. Licheng W and Ceccarelli M. A numerical simulation for design and operation of an underactuated finger mechanism for LARM hand. *Mech Based Des Struc* 2009; 37: 86–112.
22. Shuangji Y, Licheng W, Ceccarelli M, et al. Analysis and optimal design of a modular underactuated mechanism for robot fingers. In: *IEEE/RSJ international conference on intelligent robots and systems*, St. Louis, MO, 10–15 October 2009, pp.2391–2396. New York: IEEE.
23. Omarkulov N, Telegenov K, Zeinullin M, et al. Design and analysis of an underactuated anthropomorphic finger for upper limb prosthetics. *Conf Proc IEEE Eng Med Biol Soc* 2015; 2015: 2474–2477.
24. Birglen L and Gosselin CM. Kinetostatic analysis of under-actuated fingers. *IEEE T Robotic Autom* 2004; 20: 211–221.
25. Laliberte T and Gosselin CM. Simulation and design of underactuated mechanical hands. *Mech Mach Theory* 1998; 33: 39–57.
26. Kragten GA, van der Helm FCT and Herder JL. A planar geometric design approach for a large grasp range in under-actuated hands. *Mech Mach Theory* 2011; 46: 1121–1136.
27. Cutkosky MR. On grasp choice, grasp models, and the design of hands for manufacturing tasks. *IEEE T Robotic Autom* 1989; 5: 269–279.